

# Holographic photopolymer materials: nonlocal polymerization-driven diffusion under nonideal kinetic conditions

John V. Kelly, Feidhlim T. O'Neill, and John T. Sheridan

*Department of Electronic and Electrical Engineering, University College Dublin, Belfield, Dublin 4, Ireland*

Cristian Neipp, Sergi Gallego, and Manuel Ortuno

*Departamento de Física, Ingeniería de Sistemas y Teoría de la Señal, Departamento Interuniversitario de Óptica, Universidad de Alicante, Apartado 99, E-03080 Alicante, Spain*

Received January 23, 2004; revised manuscript received May 21, 2004; accepted August 6, 2004

The kinetics of photosensitive polymer holographic recording materials are examined assuming a material that exhibits nonideal kinetic behavior. Previously, a linear relationship between monomer concentration and polymerization was assumed when deriving the nonlocal polymer-driven diffusion (NPDD) model. This is consistent with ideal kinetic conditions in which chain termination is governed by a bimolecular process. However, these models have been reported to disagree with experimental results. In a limiting case of nonideal kinetics it is assumed that primary termination is dominant. In this case the NPDD model must be modified to incorporate a quadratic relationship between the monomer concentration and the polymerization rate. By use of a multiharmonic expansion method of solution the predictions of ideal (bimolecular or linear) and nonideal (primary or quadratic) kinetic models are compared. By using these models we carried out numerical fits to experimental growth curves of gratings recorded in an acrylamide-based cross-linked photopolymer system. Superior fits are achieved by use of the primary termination model. Physical parameters such as the diffusion constant are extracted and compared with results previously reported in the literature. © 2005 Optical Society of America

OCIS codes: 050.7330, 090.2900, 090.2890, 050.2770.

## 1. INTRODUCTION

Photopolymers have received much attention recently for use as holographic recording media.<sup>1,2</sup> Since photopolymers are self-processing, their potential as data storage media is also becoming a reality.<sup>3</sup> Therefore the need for an accurate model of the photochemical process involved has never been more critical.

Zhao and Mouroulis<sup>4</sup> developed a one-dimensional diffusion model that accounts for low spatial frequency cut-off and reciprocity failure; we refer to this model as the polymerization-driven diffusion model. An extension of this model, the nonlocal polymerization-driven diffusion (NPDD) model,<sup>5–7</sup> includes a parameter  $\sigma$  that quantifies the nonlocal medium response that arises because of chain growth and that has been used to explain high spatial frequency cutoff. According to the NPDD model the material behavior is governed by several physical variables including diffusion constant  $D$  of the monomer and polymerization rate  $F$ . These were previously determined for different materials by carrying out a multidimensional least-squares fit to experimental results in conjunction with Kogelnik's two-wave coupled-wave theory<sup>8</sup> and the rigorous coupled-wave model.<sup>9,10</sup>

Although some of these parameters are difficult to determine independently, some progress has been made in experimentally determining others. The refractive-index modulation, for example, can be determined from first

principles by use of the Lorentz–Lorenz formula if the refractive indices of the polymer and the monomer are known individually.<sup>11</sup> Furthermore, Moreau *et al.* proposed that the initial diffusion constant of the material can be estimated using short exposures.<sup>12</sup> Several other parameters remain to be independently determined, for example,  $\alpha$ , which describes the variation of the diffusion constant during exposure,<sup>4</sup> and  $\gamma$ , which determines the nonlinear relationship between exposure intensity and polymerization.<sup>13</sup> The polymerization rate in the NPDD model is defined as

$$F_0 = \kappa I_0^\gamma(x), \quad (1)$$

where  $I_0$  is the illuminating intensity and  $\gamma$  and  $\kappa$  are assumed to be constants. In a previous study<sup>6</sup> the NPDD was derived, following the analysis of Odian,<sup>14</sup> and Kwon *et al.*,<sup>13</sup> assuming that the rate of polymerization is proportional to the square root of the illuminating intensity, i.e.,  $\gamma = 0.5$ , and is linearly proportional to monomer concentration. However, based on experimental observations it has been reported that the value of  $\gamma$  can range between  $0.5 < \gamma < 1.5$ .<sup>14,15</sup> Based on experimental observations<sup>6,16</sup> it has also been noted that the rate of polymerization changes throughout the course of each exposure. In one previous publication<sup>6</sup> it was reported that, when fitting growth curves by use of a polynomial technique at the start of exposure, the resulting  $\kappa$  value was

found to be approximately ten times greater than the value estimated when fitting the full growth curve by use of the least-squares technique. Following discussion with others in this field, we further note that this behavior has been observed in several materials and that the rate of polymerization appears to decrease to zero as exposure time varies to infinity.<sup>16</sup>

One of the most fundamental mechanisms that remain to be fully explained is the relationship between the rate of polymerization and the concentrations of monomer, polymer, dye, and initiator. To date in the derivation of the NPDD<sup>6</sup> it has always been assumed that a bimolecular termination process governs the rate of polymerization. In this case most termination is due to polymer chains terminating other chains, and a linear relationship is shown to exist between monomer concentration and the polymerization rate. In certain materials, however, this linear relationship does not always exist.<sup>14,17</sup>

First we review the photochemical process involved in grating formation and in particular examine the assumptions made in the derivation of the polymerization rate given in Eq. (1). We argue that in the highly constrained environment of a photopolymer dry layer, termination is much more likely to arise through the mechanism of primary termination in which immobilized polymer chains are terminated by monomer radicals. Based on this assumption we present a nonideal kinetic analysis and describe the required generalization of the NPDD model. The resulting NPDD equations are solved numerically for both the bimolecular (ideal) and primary (nonideal) cases and the effects of the chain termination mechanism are examined.

These two models are then used to extract physical parameters by use of a multidimensional nonlinear fitting algorithm. To provide a consistent comparable set of results the identical sets of experimental data as used in previous papers<sup>5,6</sup> are again employed. The resulting estimates of material parameters  $D$ ,  $\sigma$ , and  $\kappa$  are presented for both models and are compared to previous estimates in the literature. It is found that the NPDD results based on primary termination provide superior fits to experimental data than those based on bimolecular termination.

## 2. MODELING THE PHOTOCHEMICAL PROCESSES

Here, following the general form and notations of the analysis presented in Refs. 6, 13, and 14, we first discuss the case of radical chain polymerization under ideal kinetics involving bimolecular termination. In particular we examine polymerization that is due to photoinitiation. In Section 3 we then discuss some possible causes of deviation from ideal kinetic behavior including the limiting case of primary termination.

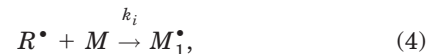
Free radical polymerization is a chain reaction that involves three main steps, namely, initiation, propagation, and termination. Initiation first involves the production of free radicals



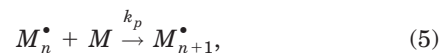
where  $k_d$  is the radical generation rate constant. The rate of this reaction is given by

$$R_d = d[R^\bullet]/dt = k_d[I], \quad (3)$$

where  $[R^\bullet]$  is the free radical concentration and  $[I]$  is the initiator concentration. The free radicals then bind to a monomer  $M$  to form the chain-initiation species  $M_1^\bullet$ :



where  $k_i$  is the initiation rate constant. The radical  $M_1^\bullet$  then propagates by bonding with other monomer molecules to form a long polymer chain with an active tip known as a macroradical:



where  $k_p$  is the propagation rate constant. Due primarily to the cage effect<sup>14</sup> only a fraction  $f$  of radicals react with a monomer in the start reaction. The rate of radical formation is then given by

$$R_r = fk_d[I]. \quad (6)$$

Monomer radicals are generated at a rate

$$R_i = d[M_1^\bullet]/dt = k_i[R^\bullet][M], \quad (7)$$

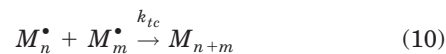
where  $[M]$  is the monomer concentration and  $[R^\bullet]$  is the primary radical concentration.  $R_i$  is much greater than  $R_d$ , therefore initiator radicals are consumed as fast as they are generated. The rate-determining step is thus the initiator decomposition. Initiator radicals are consequently formed with a rate of

$$d[R^\bullet]/dt = fk_d[I] - k_i[R^\bullet][M] = 0. \quad (8)$$

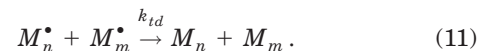
The rate of the chain initiation reaction is therefore

$$R_i = k_i[R^\bullet][M] = fk_d[I]. \quad (9)$$

Propagation would continue until the supply of monomer is exhausted were it not for the strong tendency of radicals to react in pairs to form a paired-electron covalent bond with loss of radical activity. At sufficiently low initiator concentrations, termination occurs mainly by combination<sup>14</sup>



or by disproportionation<sup>14</sup>



Therefore the termination rate is given by

$$R_t = k_t[M^\bullet]^2, \quad (12)$$

where  $k_t$  is the termination constant that represents the summation of  $k_{tc}$  and  $k_{td}$  and  $[M^\bullet]$  is the total concentration of all the chain radicals of size  $M_1^\bullet$  and larger.<sup>14</sup> For low monomer conversions we assume that the rate of radical formation equals the rate of radical disappearance (Bodenstein steady-state principle).<sup>14</sup> Also at low monomer conversions, only a little monomer is used up and

$[I] \approx [I_0]$ . Reaching steady state implies that the rate of initiation  $R_i$  and the rate of termination  $R_t$  are equal, giving

$$fk_d[I] = k_t[M^\bullet]^2. \quad (13)$$

Solving for  $[M^\bullet]$  we obtain

$$[M^\bullet]_{\text{stat}} = (fk_d[I]/k_t)^{1/2}. \quad (14)$$

Assuming much more monomer is consumed because of propagation than is consumed in the initiation reaction, the propagation rate approximates the polymerization rate, which is given by

$$R_p = -d[M]/dt = k_p[M^\bullet][M], \quad (15)$$

substituting from Eq. (14) for  $[M^\bullet]$ :

$$R_p = k_p(fk_d/k_t)^{1/2}[I]^{1/2}[M]. \quad (16)$$

Equation (16) reveals that, under ideal kinetic conditions,<sup>18</sup> the propagation rate is linearly proportional to monomer concentration and is proportional to the square root of the initiator concentration. In the case of photochemical formation of free radicals there are a number of initiation mechanisms.<sup>19</sup> Many involve a photochemical electron transfer reaction. The initiator consists of dye and a reducing agent. An excited dye molecule accepts an electron from the reducing agent, i.e., a tertiary amine that then becomes a free radical. The initiation rate can be given by

$$R_i = f\Phi' I_a, \quad (17)$$

where  $\Phi'$  is the number of radicals produced per photon absorbed and  $f$  is the initiator efficiency.<sup>14</sup>  $I_a$  is the intensity of light absorbed in moles of light quanta per liter per second. Given that the spatially modulated illumination is  $I(x) = I_0[1 + V \cos(Kx)]$ :  $V$  is the visibility, the grating vector magnitude  $K = 2\pi/\Lambda$ , and  $\Lambda$  is the grating period. Therefore

$$I_a(x) = I(x)[1 - \exp(-\epsilon Z d)] = I(x)(1 - T), \quad (18)$$

where  $\epsilon$  is the molar absorptivity,  $Z$  is the concentration of the photosensitizers,  $d$  is the photopolymer layer thickness, and  $T$  is the transmittance of the layer. The concentration of free radicals is then given by

$$[M^\bullet] = \left[ \frac{f\Phi' I(x)(1 - T)}{k_t} \right]^{1/2}. \quad (19)$$

Therefore the polymerization rate is given by

$$R_p = k_p[M] \left[ \frac{f\Phi' I(x)(1 - T)}{k_t} \right]^{1/2}. \quad (20)$$

$\kappa$  is defined as  $k_p\{[\Phi(1 - T)]/k_t\}^{1/2}$ , where  $\Phi = f\Phi'$ , which is the basis of the NPDD model presented in Ref. 6.

Examining Eq. (16) we observe that the propagation rate is proportional to the square root of initiator concentration  $R_p \sim [I]^{1/2}$ . Intensity does not appear explicitly because we discuss just the chemical process. Assuming a photochemical process (photoinitiation), from Eq. (20) we observe that the propagation rate is predicted to depend on the square root illuminating intensity,  $R_p \sim \sqrt{I(x)(1 - T)}$ . Therefore there is an intimate relationship between initiator concentration and illuminating

intensity. Comparison of these equations shows that  $k_d$ , the rate constant for the production of free radicals in Eq. (16), is related to parameter  $\Phi'$  in Eq. (20). Based on this observation and assuming both steady-state conditions and ideal kinetics, the rate of propagation for free radical polymerization has the form

$$R_p = \text{constant} \times [M] \cdot l^{1/2}, \quad (21)$$

where we introduce parameter  $l$ , which now represents the effects of both light intensity and initiator concentration. However, as we indicated in Section 1, experimental results<sup>6,15,16</sup> show deviations from this relationship and the powers to which each of the above terms is raised seem to vary. In fact it is known that in the most general case the propagation rate is of the form<sup>14,15</sup>

$$R_p = \text{constant} \times [M]^\beta \cdot l^\gamma. \quad (22)$$

Equation (22) governs general nonideal kinetic behavior. To our knowledge no general discussion of this case has appeared within the context of photopolymer holographic materials.

### 3. NONIDEAL KINETIC BEHAVIOR

Several different special cases or regimes of nonideal kinetic behavior have been examined in the literature.<sup>14,15,18</sup> In some limiting cases it is possible to determine approximate models for suitable values (or ranges of values) of  $\beta$ . We now examine two particular cases.

#### A. Rate of Polymerization as a Function of Polymer and Monomer Concentration

The termination rate has been shown in some instances<sup>14,17</sup> to vary throughout the course of polymerization. As chain growth proceeds the increasing viscosity is thought to limit the rate of termination. The larger macroradicals cannot find or locate other radicals to terminate with, because of slowing diffusion, as easily as they can find monomers to propagate with. This causes an autoacceleration of the polymerization rate known as the gel or Trommsdorff effect.<sup>18</sup> The rate finally decreases because of the reduction in monomer concentration and severe diffusional limitations caused by vitrification. These effects have been observed in many photopolymer materials.<sup>6,14</sup> We illustrate this situation in Fig. 1.<sup>20</sup>

We note that in Fig. 1 the time scale shown on the horizontal axis might not be linear. In other words, we might

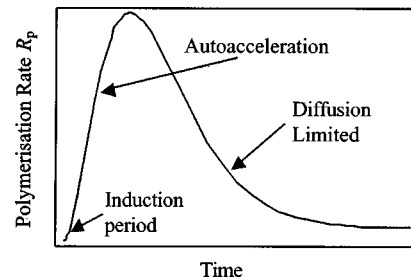


Fig. 1. Variation in the polymerization rate as a function of time (arbitrary units).

expect the time constants associated with the rise and fall to be considerably different. For cross-linked polymers, the reaction is found to reach the gel stage quickly.<sup>21</sup> If we assume this to be the case, then we will have a brief induction and autoacceleration period with monomer concentration being the dominant parameter that affects the polymerization rate throughout the reaction. We believe that this dependence can be described in terms of a chain termination mechanism that we now discuss.

### B. Effects of Chain Termination Mechanism

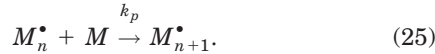
Recall that termination of propagating chains can occur through two mechanisms. First, bimolecular termination, in which two propagating radicals diffuse until they are in close proximity and then rearrange themselves until they are sufficiently close for chemical reaction. Second, primary termination, in which propagating radicals are terminated by reaction with primary radicals.<sup>14</sup>

When diffusion of propagating chains is restricted, as would be the case in a cross-linked polymer, or when we have a relatively high concentration of mobile initiator, primary termination becomes the dominant mechanism. This could be the dominant mechanism for termination in many dry photopolymer layer materials in which movement of chains is highly constrained. Therefore let us examine the case of radical chain polymerization with exclusive primary termination in detail.

#### (i) Initiation

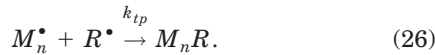


#### (ii) Propagation



#### (iii) Termination

Whereas in the ideal case we had termination by bimolecular termination, expressions (10) and (11), we now have



Writing the rate equations for the three stages we have

$$R_i = k_i[R^\bullet][M], \quad (27)$$

$$R_p = k_p[M^\bullet][M], \quad (28)$$

$$R_{tp} = k_{tp}[M^\bullet][R^\bullet], \quad (29)$$

where  $k_{tp}$  is the termination constant that is due to primary termination. As in the analysis in Section 2 we again assume steady-state conditions that imply that the rate of initiation  $R_i$  and the rate of termination  $R_{tp}$  are equal. Therefore, by combining Eqs. (27) and (29) we can determine the macroradical concentration

$$[M^\bullet] = \frac{k_i}{k_{tp}}[M], \quad (30)$$

and substituting this into Eq. (28) yields

$$R_p = \frac{k_p k_i [M]^2}{k_{tp}}. \quad (31)$$

From Eq. (31) it can be seen that, in the extreme case when all termination is by primary termination, the propagation rate is independent of initiator concentration but related to the monomer concentration raised to the second order. We would also expect primary termination to lead to a reduction in initiator efficiency  $f$  with radicals being used up in the termination process. Here, any such change is accounted for by the  $\kappa$  term as  $f$  is lumped in as a part of this parameter. Although we would not realistically expect all terminations to occur by primary termination, when the polymer chain movement is highly constrained this result would indicate that, in some photopolymer materials,<sup>14</sup> there is a greater dependence of polymerization rate on monomer concentration.

## 4. GENERALIZATION OF THE NONIDEAL POLYMERIZATION-DRIVEN DIFFUSION MODEL

The NPDD model must be revised to include a variable dependence of polymerization rate on monomer concentration. From the analysis in Section 2 we can write a generalized form of Eq. (20):

$$R_p = -\frac{\partial[M]}{\partial t} = k_p[M]^\beta \left( \frac{f\Phi'I(x)(1-T)}{k_t} \right)^\gamma. \quad (32)$$

Combining this with the diffusion equation<sup>6</sup> gives

$$-\frac{\partial[M]}{\partial t} = D \frac{\partial^2[M]}{\partial x^2} + Q[1 + V \cos(Kx)]^\gamma [M]^\beta, \quad (33)$$

where

$$Q = k_p \left( \frac{\Phi I_0 (1-T)}{k_t} \right)^\gamma. \quad (34)$$

In standard notation<sup>6</sup> the general one-dimensional NPDD equation that governs the evolution of the monomer concentration distribution becomes

$$\begin{aligned} \frac{\partial u(x, t)}{\partial t} = & \frac{\partial}{\partial x} \left[ D(x, t) \frac{\partial u(x, t)}{\partial x} \right] \\ & - \int_{-\infty}^{+\infty} \int_0^t R(x, x'; t, t') F(x', t') \\ & \times [u(x', t')]^\beta dt' dx'. \end{aligned} \quad (35)$$

In Eq. (35)  $u(x, t)$  is the free-monomer concentration,  $D(x, t)$  is the diffusion constant,  $F(x, t)$  is the polymerization rate, and  $R(x, x'; t, t')$  is the nonlocal response function. The nonlocal response function represents the effect of monomer concentration at locations  $x'$  and  $t'$  on the amount of material being polymerized at location  $x$



and time  $t$ .<sup>5</sup> Assuming rapid chain growth compared with other temporal effects, we can neglect the time non-locality and let the nonlocal response function be  $R(x, x')$ ,<sup>5</sup> effectively assuming an action-at-a-distance response. Here we chose a Gaussian probability distribution as the nonlocal response function given by

$$R(x, x') = \frac{1}{\sqrt{2\pi\sigma}} \exp\left[-\frac{(x - x')^2}{2\sigma}\right], \quad (36)$$

where  $\sigma$  is the normalized nonlocal response parameter.<sup>5,6</sup> The diffusion constant is defined by the expression  $D(x, t) = D_0 \exp[-\alpha F(x)t]$ , where  $D_0$  is the initial diffusion constant and  $\alpha$  is the diffusion coefficients decay parameter.<sup>4,5</sup> We now wish to compare materials whose responses are dominated by the effects of primary termination and bimolecular termination and for which  $\gamma = 1/2$ .<sup>13</sup>

The NPDD equations that govern the bimolecular termination case,  $\beta = 1$ , were derived elsewhere.<sup>5-7</sup> In previous papers we refer to  $\beta = 1$  and  $\gamma = 1$  as model I and  $\beta = 1$  and  $\gamma = 1/2$  as model II. Following the same nomenclature for model II we now refer to  $\beta = 2$  and  $\gamma = 1/2$  as model III. Carrying out a similar algebraic procedure we derive a corresponding set of governing differential equations for the case of primary termination. Assuming that four harmonics provide a sufficiently accurate approximation,<sup>6,22</sup> the monomer distribution is well described by the following four harmonic first-order coupled NPDD equations:

$$\begin{aligned} \frac{du_0(\xi)}{d\xi} = & -\frac{1}{4}\{4f_0u_0(\xi)^2 + (2f_0 + f_2)u_1(\xi)^2 \\ & + 2(f_0)u_2(\xi)^2 + 2f_0u_3(\xi)^2 \\ & + 2u_1(\xi)[(f_1 + f_3)u_2(\xi) + f_2u_3(\xi)] \\ & + 4u_0(\xi)[f_1u_1(\xi) + f_2u_2(\xi) + f_3u_3(\xi)] \\ & + 2f_1u_2(\xi)u_3(\xi)\}, \end{aligned} \quad (37)$$

$$\begin{aligned} \frac{du_1(\xi)}{d\xi} = & -R \operatorname{Ch}[\xi]u_1(\xi) - R \operatorname{Sh}[\xi]u_2(\xi) \\ & - \frac{S_1}{4}\{4f_1u_0(\xi)^2 \\ & + 3(f_1 + f_3)u_1(\xi)^2 + (2f_1 + f_3)u_2(\xi)^2 \\ & + 2(2f_0 + f_2)u_2(\xi)u_3(\xi) + 2f_1u_3(\xi)^2 \\ & + 4u_0(\xi)[(2f_0 + f_2)u_1(\xi) \\ & + (f_1 + f_3)u_2(\xi) + f_2u_3(\xi)] \\ & + 2u_1(\xi)[2(f_0 + f_2)u_2(\xi) \\ & + (f_1 + 2f_3)u_3(\xi)]\}, \end{aligned} \quad (38)$$

$$\begin{aligned} \frac{du_2(\xi)}{d\xi} = & -R \operatorname{Sh}[\xi][u_1(\xi) + 3u_3(\xi)] \\ & - 4R \operatorname{Ch}[\xi]u_2(\xi) - \frac{S_2}{4}\{4f_2u_0(\xi)^2 \\ & + 2(f_0 + f_2)u_1(\xi)^2 + 3f_2u_2(\xi)^2 \\ & + 2(f_1 + 2f_3)u_2(\xi)u_3(\xi) + 2f_2u_3(\xi)^2 \\ & + 4u_0(\xi)[(f_1 + f_3)u_1(\xi) + 2f_0u_2(\xi) \\ & + f_1u_3(\xi)] + 2u_1(\xi)[(2f_1 + f_3)u_2(\xi) \\ & + (2f_0 + f_2)u_3(\xi)]\}, \end{aligned} \quad (39)$$

$$\begin{aligned} \frac{du_3(\xi)}{d\xi} = & -3R \operatorname{Sh}[\xi]u_2(\xi) - 9R \operatorname{Ch}[\xi]u_3(\xi) \\ & - \frac{S_3}{4}\{4f_3u_0(\xi)^2 \\ & + (f_1 + 2f_3)u_1(\xi)^2 + (f_1 + 2f_3)u_2(\xi)^2 \\ & + 4f_2u_2(\xi)u_3(\xi) + 3f_3u_3(\xi)^2 \\ & + 4u_0(\xi)[f_2u_1(\xi) + f_1u_2(\xi) + 2f_0u_3(\xi)] \\ & + 2u_1(\xi)[(2f_0 + f_2)u_2(\xi) + 2f_1u_3(\xi)]\}, \end{aligned} \quad (40)$$

where  $\xi = F_0t$ ;

$$\begin{aligned} \operatorname{Ch}[\xi] = & \exp[-\alpha F_0t(\sqrt{1-V} + \sqrt{1+V})/2] \\ & \times \cosh[\alpha F_0t(\sqrt{1+V} - \sqrt{1-V})/2]; \end{aligned}$$

$$\begin{aligned} \operatorname{Sh}[\xi] = & \exp[-\alpha F_0t(\sqrt{1-V} + \sqrt{1+V})/2] \\ & \times \sinh[\alpha F_0t(\sqrt{1+V} - \sqrt{1-V})/2]; \end{aligned}$$

$S_i = \exp(-i^2K^2\sigma/2)$ ;  $u_0, u_1, u_2$ , and  $u_3$  are the monomer concentration harmonic components;  $f_0, f_1, f_2$ , and  $f_3$  are the polymerization rate harmonic components that depend on fringe visibility  $V$  and on  $\gamma$  (Ref. 6); and  $R$  in this case defines the relationship between the diffusion constant and the polymerization rate where  $R = DK^2/F_0$ . Varying  $R$  is equivalent to varying  $\alpha$ ,<sup>4</sup> therefore for simplicity we set  $\alpha = 0$  for the calculations in this paper. Note that in model II the parameters  $R$  and  $\xi$  are dimensionless. In model III, however,  $R$  and  $\xi$  are in units of mole per cubic centimeter and cubic centimeter per mole, respectively.  $\xi$  can be related to exposure energy through the expression  $\xi = \kappa I_0^*t$ . Where confusion might occur, parameters are differentiated by use of subscript II for model II and subscript III for model III.

Equations (37)–(40) can be solved numerically.<sup>5,6</sup> The polymerization concentration spatial harmonic components are then given by

$$\begin{aligned}
N_0(\xi) = & \frac{1}{4} \int_0^\xi \{4f_0 u_0(\xi')^2 + (2f_0 + f_2)u_1(\xi')^2 \\
& + 2(f_0)u_2(\xi')^2 + 2f_0 u_3(\xi')^2 \\
& + 2f_1 u_2(\xi')u_3(\xi') \\
& \times 2u_1(\xi')[f_1 + f_3]u_2(\xi') + f_2 u_3(\xi') \\
& + 4u_0(\xi')[f_1 u_1(\xi') + f_2 u_2(\xi') + f_3 u_3(\xi')]\} d\xi',
\end{aligned} \quad (41)$$

$$\begin{aligned}
N_1(\xi) = & \frac{S_1}{4} \int_0^\xi \{4f_1 u_0(\xi')^2 + (3f_1 + f_3)u_1(\xi')^2 \\
& + (2f_1 + f_3)u_2(\xi')^2 + 2(2f_0 + f_2)u_2(\xi')u_3(\xi') \\
& + 2f_1 u_3(\xi')^2 + 4u_0(\xi')[2f_0 + f_2]u_1(\xi') \\
& + (f_1 + f_3)u_2(\xi') + f_2 u_3(\xi') \\
& + 2u_1(\xi')[2(f_0 + f_2)u_2(\xi') \\
& + (f_1 + 2f_3)u_3(\xi')]\} d\xi',
\end{aligned} \quad (42)$$

$$\begin{aligned}
N_2(\xi) = & \frac{S_2}{4} \int_0^\xi \{4f_2 u_0(\xi')^2 + 2(f_0 + f_2)u_1(\xi')^2 \\
& + 3f_2 u_2(\xi')^2 + 2(f_1 + 2f_3)u_2(\xi')u_3(\xi') \\
& + 2f_2 u_3(\xi')^2 + 4u_0(\xi')[f_1 + f_3]u_1(\xi') \\
& + 2f_0 u_2(\xi') + f_1 u_3(\xi') \\
& + 2u_1(\xi')[2(f_1 + f_3)u_2(\xi') \\
& + (2f_0 + f_2)u_3(\xi')]\} d\xi',
\end{aligned} \quad (43)$$

$$\begin{aligned}
N_3(\xi) = & \frac{S_3}{4} \int_0^\xi \{4f_3 u_0(\xi')^2 + (f_1 + 2f_3)u_1(\xi')^2 \\
& + (f_1 + 2f_3)u_2(\xi')^2 \\
& + 4f_2 u_2(\xi')u_3(\xi') + 3f_3 u_3(\xi')^2 \\
& + 4u_0(\xi')[f_2 u_1(\xi') + f_1 u_2(\xi') + 2f_0 u_3(\xi')] \\
& + 2u_1(\xi')[2(f_0 + f_2)u_2(\xi') + 2f_1 u_3(\xi')]\} d\xi'.
\end{aligned} \quad (44)$$

The polymer harmonic amplitudes are found numerically. The two spatial concentrations associated with the polymer and monomer distribution give rise to a combined refractive-index distribution of the form

$$n(x, \xi) = C_p \sum_{i=0}^M N_i(\xi) \cos(iKx) + C_m \sum_{i=0}^M u_i(\xi) \cos(iKx), \quad (45)$$

where  $C_p$  and  $C_m$  are proportionality constants. In the case of longer exposures the effect of the monomer concentrations is neglected.<sup>4-6</sup>

## 5. NUMERICAL COMPARISON OF MODELS II AND III

Here we compare models II and III by using four harmonic expansions. The models are solved numerically and in each case the harmonic coefficients of monomer and polymer concentration are plotted as a function of  $\xi$ . The resulting grating profile shapes are then examined for different values of  $R$  and  $\sigma$ .

Figures 2(a) and 2(b) show the first two harmonic components of monomer concentration for models II and III, respectively. The initial rate of decrease in monomer concentration is much slower for model II than for model III although, as the concentration of  $u_0$  decreases, model III predicts that its value approaches zero more gradually than for model II. Figures 3(a) and 3(b) show the evolution of the first four harmonic components of polymer concentration. Similarly, model II predicts a slower initial growth in polymer concentration than model III, whereas model III predicts a more gradual approach toward the maximum polymer concentration value.

From Fig. 3 it can be seen that the saturation value for the  $N_1$  harmonic of polymer concentration is greater for model II than for model III. Furthermore the higher-order component saturation values are smaller for model II.

For a nonlocal material,  $\sigma > 0$ , the resulting polymer concentration profiles for model III become more sinusoidal and also less visible as the saturation value of the higher-order harmonics is suppressed; see Fig. 4. This follows the same behavior as predicted by model II.<sup>6</sup>

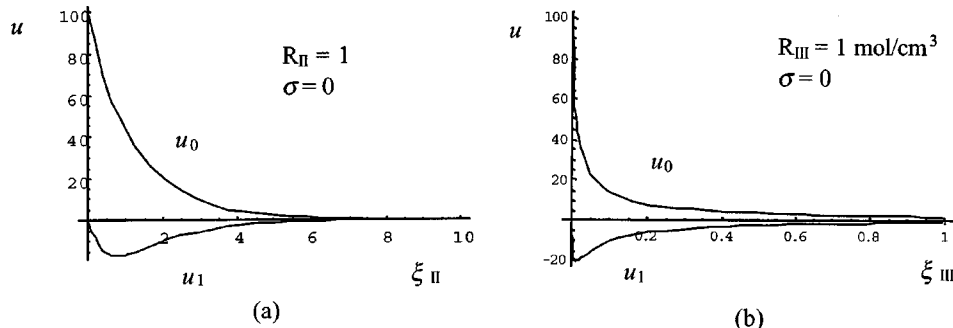


Fig. 2. Harmonic amplitudes of monomer concentration with  $\alpha = 0$  and  $\sigma = 0$ , predicted by (a) model II,  $R_{II} = 1$  and (b) model III,  $R_{III} = 1 \text{ mol/cm}^3$ .

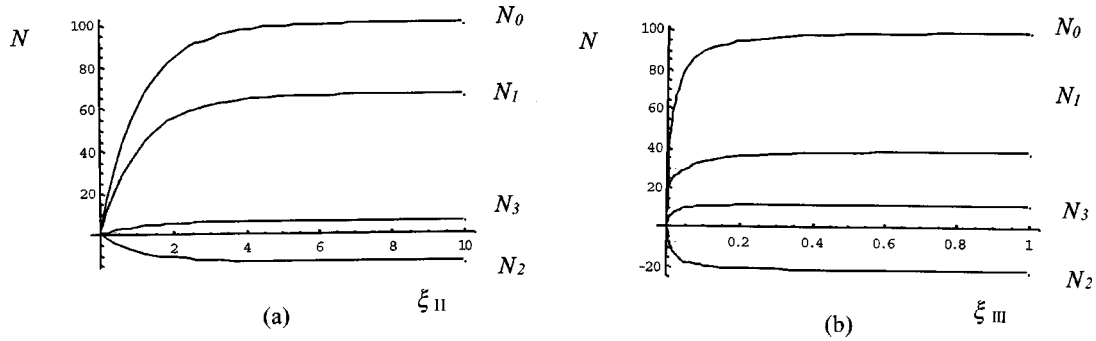


Fig. 3. Harmonic amplitudes of polymer concentration where  $\alpha = 0$  and  $\sigma = 0$  as predicted by (a) model II,  $R_{II} = 50$  and (b) model III,  $R_{III} = 50 \text{ mol/cm}^3$ .

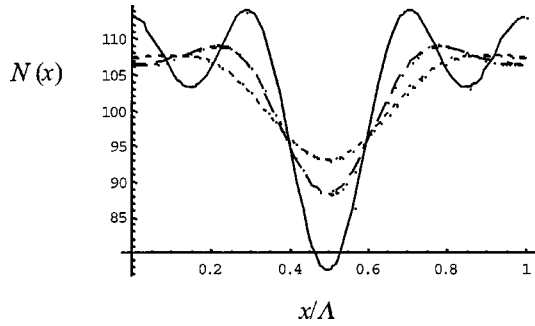


Fig. 4. Spatial distribution of polymer concentrations, where  $R_{III} = 1 \text{ mol/cm}^3$  and  $\alpha = 0.1$ . Solid curve,  $\sigma = 0$ ; long dashed curve,  $\sigma = 1/64$ ; short dashed curve  $\sigma = 1/32$ , where  $\sigma$  is the normalized nonlocal length.

## 6. LEAST-SQUARES FIT TO EXPERIMENTAL DATA

Using models II and III we now present new fits to experimental data that were previously examined in the literature.<sup>6</sup> The four coupled equations were solved numerically to determine the monomer coefficients, and refractive-index modulation  $n_1$  was then determined from the first harmonic of polymer concentration  $N_1$ , assuming a linear relationship between the change in refractive index and the polymer concentration  $n_1 = C_p N_1$ .<sup>5,6</sup> The experimental data, consisting of diffracted intensity values corrected for Fresnel reflections, were previously converted by use of the Kogelnik first-order two-wave coupled-wave model to give the first harmonic grating refractive-index modulation.<sup>23</sup> The data were then fitted by use of a least-squares algorithm in which the mean-square error (MSE) was minimized to obtain the best fit. Four experimental growth curves recorded at different spatial frequencies were used in the fitting and estimation process. The data were fitted to extract diffusion constant  $D$ , the polymerization rate constant  $\kappa$ , and both  $C_p$  and  $S$ . Basing our new results on the four data sets previously discussed in the literature is intentional. The error bars used in this paper reflect both uncertainties in our experimental system and the reproducibility of our results. The experimental setups and the sources of error have been described in detail in earlier papers.<sup>23,24</sup>

To carry out the fitting process, first search ranges of suitable values are estimated for each parameter. From previous experimental<sup>12</sup> and theoretical<sup>6,22</sup> results we expect  $D$  to lie in the search range of  $10^{-9} \text{ cm}^2/\text{s} < D$

$< 10^{-14} \text{ cm}^2/\text{s}$ . By manual iteration, search ranges for  $\kappa$  were estimated to be between  $3 \times 10^{-2} \text{ s}^{-1} \text{ mW}^{-1/2} \text{ cm} < \kappa < 9 \times 10^{-2} \text{ s}^{-1} \text{ mW}^{-1/2} \text{ cm}$  for model II and  $3 \times 10^{-4} \text{ s}^{-1} \text{ mW}^{-1/2} \text{ cm}^4 \text{ mol}^{-1} < \kappa < 9 \times 10^{-4} \text{ s}^{-1} \text{ mW}^{-1/2} \text{ cm}^4 \text{ mol}^{-1}$  for model III. To estimate the search range for the  $C_p$  parameter we used the relationship

$$C_p = \frac{n_1^s}{N_1^s}, \quad (46)$$

where  $n_1^s$  is the saturation refractive-index modulation extracted from the experimental data at steady state and  $N_1^s$  is the theoretical saturation value of the first harmonic of polymer concentration.<sup>22</sup> By examining the theoretical predictions of models II and III for  $R$  values between  $1 < R < 1000$  we estimated a range of  $N_1^s$  values between  $9 \text{ mol/cm}^3 < N_1^s < 66 \text{ mol/cm}^3$ . The  $n_1^s$  values extracted from the experimental data used were found to lie within the range of  $0.001 < n_1^s < 0.003$ . Using these two ranges of values we could confine our search for a best-fit  $C_p$  value between  $1 \times 10^{-4} \text{ cm}^3/\text{mol} < C_p < 5 \times 10^{-5} \text{ cm}^3/\text{mol}$ . Values for  $S$  were allowed to range from a purely local case in which  $S = 1$  ( $\sigma = 0$ ) to a highly nonlocal case in which  $S = 0.1$ . These  $S$  values correspond to a range for  $\sqrt{\sigma'}$ , the nonlocal response length, between  $0 \text{ nm} \leq \sqrt{\sigma'} \leq 345 \text{ nm}$ , where  $\sigma'$  is related to  $\sigma$  by the equation  $\sigma = \sigma'/\Lambda^2$ . Based on values reported in the literature<sup>6,22</sup> we might reasonably expect the nonlocal response length to be within this range.

Many numerical searches were carried out over the parameter ranges indicated and also over several combinations of subranges within those indicated. In all cases the MSE values were used to quantify the quality of the fit, i.e., the MSE was the cost function. The nature of this iterative search process does not allow us to claim with absolute certainty that the global minimum has been found. However, the number of individual searches carried out and the number of permutations of search ranges were substantial.

## 7. RESULTS: PARAMETER VALUE ESTIMATES

Fitting was carried out to growth curves for gratings, recorded in the same medium, with four different spatial frequencies. The parameters estimated for fitting both models II and III to the experimental data are shown in

Tables 1 and 2, respectively. The average values and uncertainties of the estimates for these parameters are also presented. Previously<sup>6</sup> a two harmonic expansion-based analytic expression for the  $N_1$  polymer concentration, derived by use of model II, was fit to these data. Here we use a four harmonic expansions fit with the numerical technique described in Section 6.

The average value of the diffusion constant for model II was estimated to be  $6.35 \pm 3.65 \times 10^{-11} \text{ cm}^2/\text{s}$ . This value of diffusion constant is larger than that estimated by use of model III, which was estimated to be  $0.99 \pm 0.22 \times 10^{-11} \text{ cm}^2/\text{s}$ . These values make sense in terms of the material being modeled in each. In model III we observe a highly constrained, diffusion-limited environment and therefore would expect a slower diffusion rate. We note that values for  $D$  of  $3.31 \times 10^{-14} \text{ cm}^2/\text{s}$  previously reported<sup>6</sup> differ significantly from what we determined and report in this paper. This appears to be due primarily to the use of the four harmonic model as opposed to the two harmonic analytic technique used previously. We also note that (i) many local minima can be found when attempting to determine best-fit parameters and (ii) an uncertainty of as much as  $\pm 10\%$  for the experimental data exists and increases the difficulty of locating a true global minimum.

Examining the predictions of model III, the estimated parameters generally follow previous theoretical and experimental identified trends associated with holographic recording in photopolymers. We expect the  $R$  value to increase as the period decreases, following the relationship  $R \propto 1/(I_0^{1/2} \Lambda^2)$ . We note that, from the experimental results, the  $R$  value is observed to increase as the period gets smaller. The  $R$  values estimated from the results for 1250 lines/mm and 2000 lines/m, which represent the largest increase between successive data sets, closely follow the expected inverse square relationship. We expect  $S$  to decrease as the period increases. We also note that the MSE values calculated for model II are generally larger than those found when fitting by use of model III.

Deviations from these general trends do occur. The diffusion constant appears to increase slightly as a function of the period. When using model III, in the 2250-lines/mm case there is an unexpectedly large increase in the value of  $\kappa$  and a correspondingly lower value of  $R$ . Similarly for the 1250-lines/mm case the quality of fit measured by use of the MSE is not as good compared with other data sets. Once again deviations could be due to the quality of the data or the fitting algorithm could in fact not have determined the global minimum during minimization of the MSE. However in Fig. 5 we show a fit to the experimental data set for the 1250-lines/mm grating. The solid curve represents the best theoretical fit obtained by use of model III and the dashed curve indicates the theoretical fit obtained by use of the mean values of the estimated parameters listed in Table 2. The error bars indicate an experimental accuracy of  $\pm 10\%$ . Clearly the mean value fit lies within this uncertainty. Therefore parameter estimates provide good fits within the range of accuracy of the experimental data.

Let us compare the values found by use of model III for the different physical parameters with comparable results that appear in the literature. Moreau *et al.*<sup>12</sup> experimentally determined the diffusion constant for short exposures in a DuPont Omnidex photopolymer to be  $6.52 \times 10^{-11} \text{ cm}^2/\text{s}$ . Although the experimental growth curves used in this paper are recorded in a different acrylamide-based system, we note that our diffusion constant value is of the same order of magnitude.

Also note that we estimate the nonlocal response length to be  $\sqrt{\sigma'} = 67 \pm 18 \text{ nm}$ , which seems to agree with results for a DuPont photopolymer reported by Wu and Glytsis<sup>22</sup> in which they estimated the nonlocal response length to be 59.27 nm. Examining the value of  $\kappa$  estimated from models II and III in this paper we observed that it is much bigger for model II than for model III. However  $\kappa_{\text{II}}$  is fundamentally different from  $\kappa_{\text{III}}$  because it has different units in each case and therefore is

**Table 1. Characteristic Parameters Extracted from Fits to Experimental Data with Model II**

Spatial Frequency (lines/mm)	$C_p$ ( $\text{cm}^3/\text{mol} \times 10^{-5}$ )	$\kappa$ ( $\text{s}^{-1} \text{ mW}^{-1/2} \text{ cm}$ )	$D_0$ ( $\text{cm}^2/\text{s} \times 10^{-11}$ )	$R$	$S$	$\sqrt{\sigma'}$ (nm)	MSE ( $\times 10^{-11}$ )
1000	3.9	0.05	3.4	1.3	0.97	39	15
1250	2.9	0.08	5	2	0.84	75	17
2000	2.8	0.056	7	10	0.72	65	50
2250	2.8	0.085	10	12	0.6	71	35
Mean	$3.1 \pm 0.8$	$0.068 \pm 0.0018$	$6.35 \pm 3.65$	6.3	0.78	$62.5 \pm 23.5$	29

**Table 2. Best-Fit Parameters Extracted from Fits to Experimental Data with Model III**

Spatial Frequency (lines/mm)	$C_p$ ( $\text{cm}^3/\text{mol} \times 10^{-5}$ )	$\kappa$ ( $\text{s}^{-1} \text{ mW}^{-1/2} \text{ cm}^4 \text{ mol}^{-1}$ )	$D_0$ ( $\text{cm}^2/\text{s} \times 10^{-11}$ )	$R$ ( $\text{mol}/\text{cm}^3$ )	$S$	$\sqrt{\sigma'}$ (nm)	MSE ( $\times 10^{-11}$ )
1000	7.1	0.00036	0.98	55	0.91	69	8.49
1250	5.4	0.00044	0.77	55	0.83	85	27
2000	3.9	0.00045	1.03	186	0.8	53	7.8
2250	3.6	0.00078	1.19	158	0.69	61	1.7
Mean	$5 \pm 2.1$	$0.0005 \pm 0.0003$	$0.99 \pm 0.22$	114	0.8	$67 \pm 18$	11



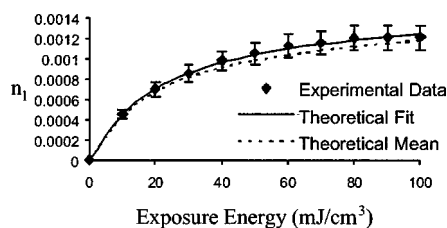


Fig. 5. Fit to experimental data by use of estimated parameters given in Table 2. Spatial frequency = 1250 lines/mm. Error bars are included to allow for the possibility of  $\pm 10\%$  experimental error.

not directly comparable. More important however is that  $\kappa_{\text{III}}$  appears to remain constant throughout the growth curve. When examining the value of  $\kappa$  for model III for exposure times close to zero, we noted almost no variation between that value and the value determined over the entire curve. This was previously determined not to be the case for model II,<sup>6</sup> which would seem to indicate that the faster initial rate of polymerization predicted by model III, which assumes primary termination, provides a more accurate representation of polymerization rate variation than that predicted by model II.

## 8. CONCLUSION

We have proposed a nonideal kinetic model of photosensitive polymer holographic recording materials that takes into account the possibility that a nonlinear relationship between monomer concentration and rate of polymerization exists within certain types of photopolymer. The nonlocal polymer-driven diffusion model (NPDD) was developed to include a quadratic relationship between rate of polymerization and monomer concentration and numerically solved by use of a four harmonic approximation. The previous ideal linear (bimolecular) model, model II, was then compared with the proposed nonideal (primary) model, model III. In this case a faster initial growth in polymer concentration followed by a more gradual saturation is predicted by model III. When comparing the quality of the fits found for both models II and III, better fits to the same sets of experimental data were achieved by use of model III. We believe our results support the conclusion that phase grating formation in cross-linked polymers involves a substantial amount of polymerization, which terminates with the primary termination mechanism. Conclusive proof of this contention has not been provided here. To determine the dominant form of termination unambiguously, many more experimental comparisons are necessary between the two models for gratings recorded in material that contains different concentrations of cross linker and initiator. We emphasize these two materials because it appears that their concentrations are the two main factors that affect the termination process.

When fitting model III to discrete sections of the experimental growth curves, the value of  $\kappa$  remains almost constant. In previous publications the value of  $\kappa$  estimated by use of model II was found to vary. In summary, model III seems to model our material more accurately and the material process appears to be governed by primary termination.

A paper by Blaya *et al.* that discusses the chain termination mechanism has been brought to our attention.<sup>25</sup> Their research involves an extensive examination of polymerization in photopolymers that utilize a primary termination model. However, the issue is dealt with in a different manner from ours; for example, the diffusion constant is assumed negligible.

We note that it is highly probable that the relationship between the rate of polymerization and the monomer concentration is not strictly linear or quadratic and that both primary and bimolecular termination could be involved at different stages of the process depending on the properties of the photopolymer material being examined. Further investigation is necessary to develop a fully generalized termination model.

## ACKNOWLEDGMENTS

The authors acknowledge the support of Enterprise Ireland, the Research Innovation Fund and Science Foundation Ireland, through the Basic Research Program. F. T. O'Neill currently holds an Embark Initiative postdoctoral research fellowship operated by the Irish Research Council for Science, Engineering and Technology.

J. T. Sheridan's e-mail address is john.sheridan@ucd.ie.

## REFERENCES

1. S. M. Schultz, E. N. Glytsis, and T. K. Gaylord, "Design, fabrication, and performance of preferential-order volume grating waveguide couplers," *Appl. Opt.* **39**, 1223–1232 (2000).
2. A. Sato, M. Scepanovic, and R. K. Kostuk, "Holographic edge-illuminated polymer Bragg gratings for dense wavelength division optical filters at 1550 nm," *Appl. Opt.* **42**, 778–784 (2003).
3. L. Dahr, A. Hale, K. Curtis, M. Schnoes, M. Tackitt, W. Wilson, A. Hill, M. Schilling, H. Katz, and A. Olsen, "Photopolymer recording media for high density holographic data storage," in *Conference Digest, Optical Data Storage 2000* (Institute of Electrical and Electronics Engineers, Piscataway, N.J., 2000), pp. 158–160.
4. G. Zhao and P. Mouroulis, "Diffusion model of hologram formation in dry photopolymer materials," *J. Mod. Opt.* **41**, 1929–1939 (1994).
5. J. T. Sheridan and J. R. Lawrence, "Nonlocal-response diffusion model of holographic recording in photopolymer," *J. Opt. Soc. Am. A* **17**, 1108–1114 (2000).
6. J. R. Lawrence, F. T. O'Neill, and J. T. Sheridan, "Adjusted intensity nonlocal diffusion model of photopolymer grating formation," *J. Opt. Soc. Am. B* **19**, 621–629 (2002).
7. J. T. Sheridan, M. Downey, and F. T. O'Neill, "Diffusion-based model of holographic grating formation in photopolymers: generalized non-local material responses," *J. Opt. A, Pure Appl. Opt.* **3**, 477–488 (2001).
8. H. Kogelnik, "Coupled wave theory for thick holographic gratings," *Bell Syst. Tech. J.* **48**, 2909–2947 (1969).
9. M. G. Moharam and T. K. Gaylord, "Rigorous coupled-wave analysis of planar-grating diffraction," *J. Opt. Soc. Am.* **71**, 811–818 (1981).
10. C. Neipp, M. L. Alvarez, S. Gallego, M. Ortuno, J. T. Sheridan, I. Pascual, and A. Beléndez, "Angular responses of the first diffracted order in over-modulated volume diffraction gratings," *J. Mod. Opt.* **51**, 1149–1162 (2004).
11. I. Aubrecht, M. Miller, and I. Koudela, "Recording of holographic diffraction gratings in photopolymers: theoretical modelling and real-time monitoring of grating growth," *J. Mod. Opt.* **45**, 1465–1477 (1998).

12. V. Moreau, Y. Renotte, and Y. Lion, "Characterization of Dupont photopolymer: determination of kinetic parameters in a diffusion model," *Appl. Opt.* **41**, 3427–3435 (2002).
13. J. H. Kwon, H. C. Hwang, and K. C. Woo, "Analysis of temporal behavior of beams diffracted by volume gratings formed in photopolymers," *J. Opt. Soc. Am. B* **16**, 1651–1657 (1999).
14. G. Odian, *Principles of Polymerization* (Wiley, New York, 1991).
15. C. R. Fernández-Pousa, R. Mallavia, and S. Blaya, "Holographic determination of the irradiance dependence of linear-chain polymerization rates in photopolymer dry films," *Appl. Phys. B: Lasers Opt.* **70**, 537–542 (2000).
16. W. L. Wilson, InPhase Technologies, 2000 Pike Road, Longmont, Colo. (personal communication, June 2003).
17. J. V. Kelly, F. T. O'Neill, J. T. Sheridan, C. Neipp, S. Gallego, and M. Ortuno, "Holographic photopolymer materials with nonlocal and nonlinear response," in *Organic Holographic Materials and Applications*, K. Meerholz, ed., *Proc. SPIE* **5216**, 127–138 (2003).
18. H.-G. Elias, *An Introduction to Polymer Science* (VCH Verlag GmbH, Weinheim, Germany, 1997).
19. W. J. Tomlinson, "Organic photochemical refractive-index systems," in *Advances in Photochemistry*, Vol. 12, G. S. Hammond, K. Gollnick, and J. N. Pitts, eds. (Wiley, New York, 1980).
20. E. El-Sheikh, C. Penny, F. Bakomska, R. Liu, A. Kamel, and J. Sticken, "Intelligent tutoring for polymer composite molding," presented at the Symposium on Low-Cost, High Speed Polymer Composites Processing, Michigan State University, Lansing, Mich., June 1, 1997, [http://islnotes.cps.msu.edu/trp/back/fre\\_gel.html](http://islnotes.cps.msu.edu/trp/back/fre_gel.html).
21. P. Munk, *Introduction to Molecular Science* (Wiley, New York, 1989).
22. S.-D. Wu and E. N. Glytsis, "Holographic grating formation in photopolymers: analysis and experimental results based on a nonlocal diffusion model and rigorous coupled-wave analysis," *J. Opt. Soc. Am. B* **20**, 1177–1188 (2003).
23. J. R. Lawrence, F. T. O'Neill, and J. T. Sheridan, "Photopolymer holographic recording material parameter estimation using a nonlocal diffusion based model," *J. Appl. Phys.* **90**, 3142–3148 (2001).
24. F. T. O'Neill, J. R. Lawrence, and J. T. Sheridan, "Automated recording and testing of holographic optical element arrays," *Optik (Stuttgart)* **111**, 459–467 (2000).
25. S. Blaya, L. Carretero, R. F. Madrigal, M. Ulibarrena, P. Acebal, and A. Fimia, "Photopolymerization model for holographic gratings formation in photopolymers," *Appl. Phys. B: Lasers Opt.* **77**, 639–662 (2003).